

## Microstructure, shape, stability and melting in embedded nanoparticles

*K. Chattopadhyay AND V. Bhattacharya*

Abstract | The present article reviews some of the current work on a new class of materials which are nanoscale granular materials. We shall discuss in this paper two phase granular materials where one of the phases having nanometric dimension is embedded in a matrix of larger dimension. Known as nanoembedded materials, nanocomposites or ultrafine granular materials, this class of materials has attracted attention because of the opportunity of basic studies on the effect of size and embedding matrix on transformation behaviors as well as some novel properties, which include structural, magnetic and transport properties. These are in addition to the tremendous interests in what is known as quantum structures (embedded particles size less than 5 nm) for the case of semiconductors, which will not be discussed here. We shall primarily review the work done on metallic systems where the dispersed phases have low melting points and borrow extensively from the work done in our group. The phase transformations of the embedded particles show distinctive behavior and yield new insights. We shall first highlight briefly the strategy of synthesis of these materials by non-equilibrium processing techniques, which will be followed by examples where the effect of length scales on phase transformation behaviors like melting and solidification are discussed.

### 1. Introduction

Nanostructured materials can be defined as those materials, which exhibit microstructure having the characteristic length scale of the order of a few nanometers in one or more dimensions.<sup>1</sup> Nanostructured materials can be divided into three categories.<sup>2</sup> The first category comprises materials and/or devices with reduced dimensions and/or dimensionality in the form of (isolated, substrate-supported or embedded) nanometer sized particles, thin wires or thin films. The second category comprises materials and/or devices in which the nanometer-sized microstructure is limited to a thin (nanometer sized) surface region of a bulk material. The third category consists of bulk solids with a nanometer-scale microstructure.

In this review, we shall focus on the third category of materials where nanometric second phase is embedded in a matrix.

#### 1.1. *Effects controlling the properties of nanoembedded materials*

The properties of nanoscaled materials are different from that of bulk materials due to the changes in size, atomic configuration and chemical structure. We will briefly discuss the different factors that lead to these changes.

##### 1.1.1. *Size effect*

The most obvious effect of reducing the particle size is the increase in the area of surfaces and interfaces including grain boundary areas per

Department of Materials  
Engineering, Indian  
Institute of Science,  
Bangalore 560012, India

unit volume. The atoms lying at the surfaces or interfaces have different environment both in terms of coordination and chemistry since the structure of these boundaries is significantly different from that of the bulk crystal. The structure depends on orientation of the neighboring grains and interaction of the atomic potentials across the boundaries. The end result is a more open structure with local variation. Such a structure is also subjected to a relaxation process as the atoms try to arrive at a lower energy configuration. This difference in structure and chemistry of the boundary phases become important at nanoscale since the boundary volume increases significantly with the reduction in size of the particles. The above reasoning is equally applicable to free particles as well as for nanoembedded particles. One can estimate the volume fraction of the embedded particle interface regions by assuming initially a geometrical shape and a reasonable thickness of the boundary where the effect of interactions of the potentials of different grains is significant. For the embedded case the amount of this boundary phase will also depend on the volume fraction of these materials. The material therefore behaves like a two-phase composite and depending on the property of the boundary, can yield novel properties.

In case size of the particles is reduced such that the critical length scale of physical phenomena (viz. mean free path of electrons, coherence length) becomes comparable to the characteristic microstructural length scale, size seems to play a key role in dictating the properties of such materials. For example the band spacing is expected to expand at small confinement and magnetocrystalline anisotropy can get evened out leading to a more isotropic behavior. At small size, one can observe significant changes in the alloying behavior. This leads not only to a change in the chemistry of the phases present but also their structures. We will present in brief some of the recent results highlighting this scenario in the subsequent sections

#### 1.1.2. Atomic configuration

The changes in the atomic structure result if a high density of incoherent interfaces or other lattice defects such as dislocations and vacancies are present. The cores of lattice defects represent a constrained state of solid matter structurally different from (unconstrained) crystals and/or glasses. As a consequence, a solid containing a high density of defect cores differs structurally from a defect-free solid with the same (average) chemical composition.<sup>3</sup>

Alloying behavior and hence chemical nature of nanostructured materials can differ substantially

from that of the bulk. There are reports of formation of solid-solution in systems which exhibit complete immiscibility. Even if the constituents are immiscible in the crystalline and/or molten state (e.g. Fe and Ag) the formation of solid-solution has been observed.<sup>4</sup> In semicrystalline polymer<sup>5</sup>, formation of crystalline and non-crystalline regions differing in molecular structure and/or chemical compositions at small length scale has been reported. The change in chemical nature has obvious influence on properties of these materials.

## 2. Nanoembedded metal particles

### 2.1. Synthesis

There exists several synthesis routes by which nanoembedded particles of metals and alloys can be manufactured. In the following sections we briefly summarize some of the more popular techniques used in recent time.

#### 2.1.1. Rapid Solidification

One of the popular techniques to synthesis nanoembedded metallic particles is rapid solidification.<sup>6,7</sup> This processing technique involves achievement of high cooling rate in the range  $10^{-4}$  to  $10^{-7}$  K/s, and large undercooling of the melt that leads to large departure from the equilibrium conditions. The process involves the ejection of a stream of molten metal/alloy into a thin layer or fine droplets, which is brought in intimate contact with a cooling medium (solid substrate). The heat transfer is primarily by conduction through a solid substrate. The primary requirements for the synthesis of nanomaterials from liquid are achievement of high nucleation rate and low growth rate of the solid phases involved in the liquid-solid phase changes.<sup>8</sup> The high nucleation rate can be achieved by increasing the undercooling and kinetically avoiding the heterogeneous nucleation sites. The principle of rapid solidification synthesis of embedded nanomaterials incorporates two major steps. In the first step, the dispersed phase should nucleate in the melt with a high nucleation rate and low growth rate. In the second step, the matrix phase should nucleate and grow at a very high growth velocity enabling the trapping of the dispersed solid phase co-existing in the melt.<sup>8,9</sup>

#### 2.1.2. Mechanical alloying

Mechanical Alloying is a solid-state processing technique where mechanical energy is used to drive the system away from the equilibrium. This results in the development of highly nonequilibrium structures and microstructures. One of the ways the mechanical energy that is imparted on the sample can be stored is by creating a very large

number of interfaces. This results in the reduction of the scale of the microstructures. The physical mechanisms responsible in case of ductile materials are repeated fracture, welding and re-welding of powder particles. For brittle materials the process of fracture dominates the process although the actual mechanism is less clearly understood. The process was originally developed to produce oxide dispersion strengthened (ODS) nickel and iron based superalloys for aerospace industry.<sup>10</sup> In recent time, mechanical alloying has been used to synthesize a variety of equilibrium and non-equilibrium alloy phases. The non-equilibrium phases synthesized include supersaturated solid solutions, amorphous alloys, metastable crystalline and quasicrystalline phases and nanostructured materials.<sup>11–13</sup> Recent review on mechanical alloying (Koch<sup>14</sup> and Suryanarayana<sup>15</sup>) shows that the process has been used extensively to synthesize nanocrystals of pure metals and alloys.

### 2.1.3. Solgel

The evolution of colloidal solutions with rigidity (gel) from a liquid like mixture of alkoxides and inorganic salts in a common solvent, which does not have the ability to resist shear stress (sol), is the essence of sol-gel route.<sup>16</sup> The technique gradually became known as sol-gel process because of the sudden characteristic change of viscosity at the onset of gel transition.<sup>16–18</sup> The gel can be selectively reduced to generate embedded nanoparticles.

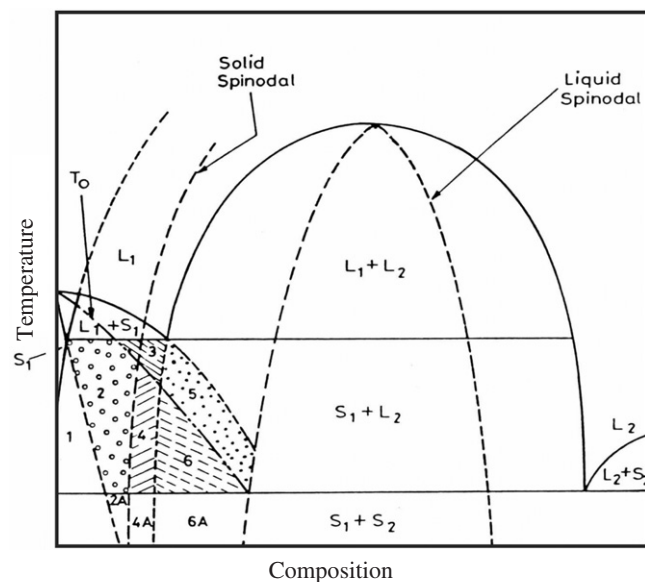
Bhattacharya et al.<sup>19,20</sup> have synthesized dispersion of lead in silica and alumina matrix by this method. In the case of silica the matrix is glassy while in case of alumina we have ultra fine alumina as the matrix. In both cases, the dispersions of lead are of 10–20 nm in size.

In addition to these, physical vapor deposition, chemical vapor deposition, inert gas condensation, ion implantation and laser beam treatments and precipitation from the vapor, from supersaturated liquids or solids (both crystalline and amorphous) appear to be techniques most commonly used to synthesize nanomaterials.

### 2.2. Development of nanodispersed microstructure during rapid solidification of an alloy melt in monotectic binary alloy melt

The monotectic system is extensively used to synthesize nano embedded particles of materials and alloys. Since this class of materials constitutes the main subject matter of this review, we elaborate the microstructure evolution pathway in these cases<sup>21</sup>. A generic discussion of the free energy curves of system exhibiting liquid miscibility gap and some of its special features is due to Cahn.<sup>22</sup> Figure 1 shows schematic of a typical monotectic phase diagram with all possible metastable extensions. When the alloy is cooled rapidly from a single-phase liquid, depending on the composition i.e. hypomonotectic, hypermonotectic or monotectic, the process of microstructure development can be different. The discussion below is restricted to those in the low volume fraction regime of the dispersed phase because of the interest in developing a microstructure with fine dispersions of low melting metals and alloys in a high melting metal matrix. When the alloy melt is cooled through the immiscible domain (hypermonotectic composition), the liquid (L) phase separates into two liquids ( $L_1+L_2$ ). Depending on the melt composition, two possibilities exist which govern the kinetics of this phase separation. Spontaneous decomposition of liquid ( $L \rightarrow L_1+L_2$ ) occurs if the melt is cooled through the spinodal domain. However, if the melt is in binodal domain the phenomena is one of nucleation and growth of  $L_2$  from the melt. As the temperature decreases continuously, primary solid phase ( $S_1$ ) nucleates below the monotectic temperature ( $T_m$ ) and the S/L interface moves at a very high velocity thereby trapping  $L_2$  within it. The size of the phase separated liquid ( $L_2$ ) droplets in the melt is dictated by the growth and coarsening rate and the time available before they are trapped by the growing solid ( $S_1$ ). In addition to the purely diffusional growth, the collisions of

Figure 1: A typical monotectic phase diagram showing all the metastable extensions.



the different particles also play a major role in the coarsening process. As pointed by Uhlman et al.<sup>23</sup> the critical velocity required for the growing solid to trap the droplets is inversely proportional to the size of the droplet. As the growth velocity of the solid depends on the amount of the undercooling achieved during rapid solidification, higher cooling rate is required to synthesize finer dispersions. The particles that are not trapped ultimately get engulfed at the grain boundaries creating a network of particles decorating the grain boundaries. This is more prominent at lower cooling rate. With very high cooling rate, it is also possible to suppress the decomposition of liquid in the immiscible liquid domain if the liquid does not enter the limit given by the spinodal regime. The liquid in such a case can kinetically avoid the process of nucleation and may enter the domain below the equal free energy curve  $T_0$  between the melt and the solid (region 6). In this domain, it is kinetically possible to achieve solidification without partitioning leading to the formation of highly transient metastable solid solution. This solid will decompose spontaneously to yield a nanodispersed microstructure.<sup>24</sup> The size distribution in this case is narrower compared to the liquid phase separation route due to the large driving force for nucleation from the highly metastable solid solution and relatively slower diffusion in the solid state. In many cases, both the liquid trapping

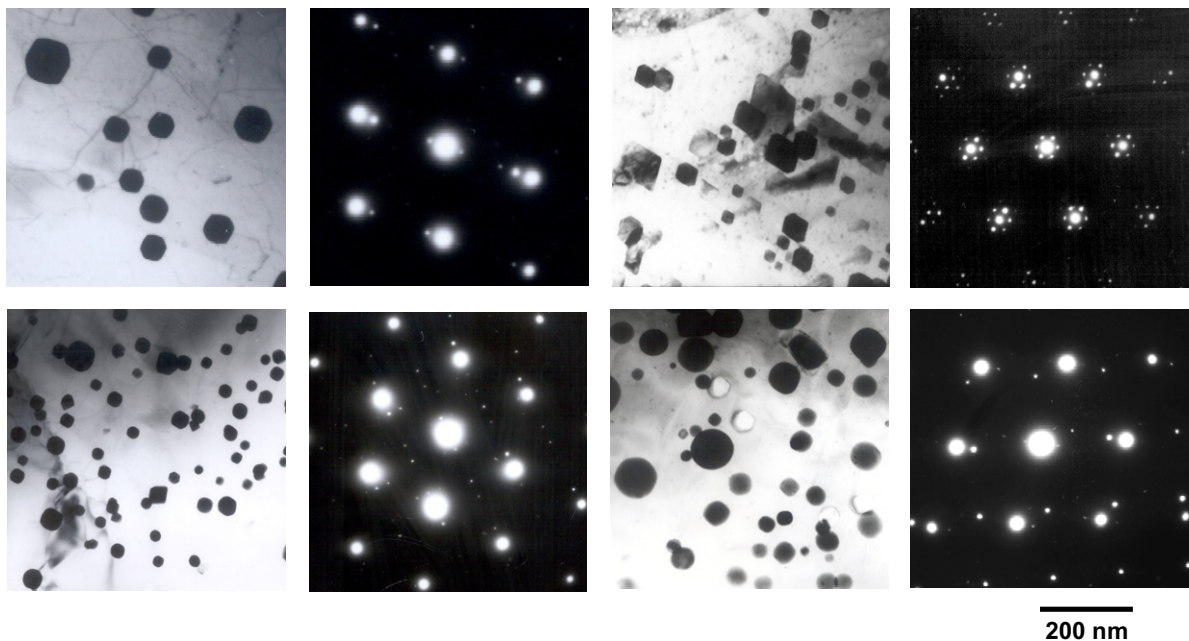
and the decomposition of the metastable solid can occur simultaneously. The microstructure under such a processing condition is characterized by a bimodal distribution of very fine dispersoids due to the solid state decomposition and the coarser distribution of particles through the trapping of the phase separating second liquid ( $L_2$ ) by the moving interface.

### 2.3. Evolution of shape

#### 2.3.1. Shape of nanoparticles

Due to the shorter diffusion distances in nanoparticles, the particles exhibit equilibrium shapes. The projected shapes of the nanodispersed particles can be obtained from the bright field transmission electron microscopic images along prominent zone axes of the matrix. The shapes of Pb, In, Bi and Sn viewed along [011] zone axis of Al matrix is shown in figure 2. The corresponding diffraction pattern is also shown in the same figure. From the projected images along prominent zone axes, it is possible to reconstruct the actual three dimensional (3d) shapes of the dispersoids. Experimental observation suggests that the shape of the particles conform to cubeoctahedral symmetry with sharper 111 and 100 facets for both Pb and metastable cubic In (see figures 2a and 2b). However, in the case of Bi and Sn a spectrum of shapes could be observed.

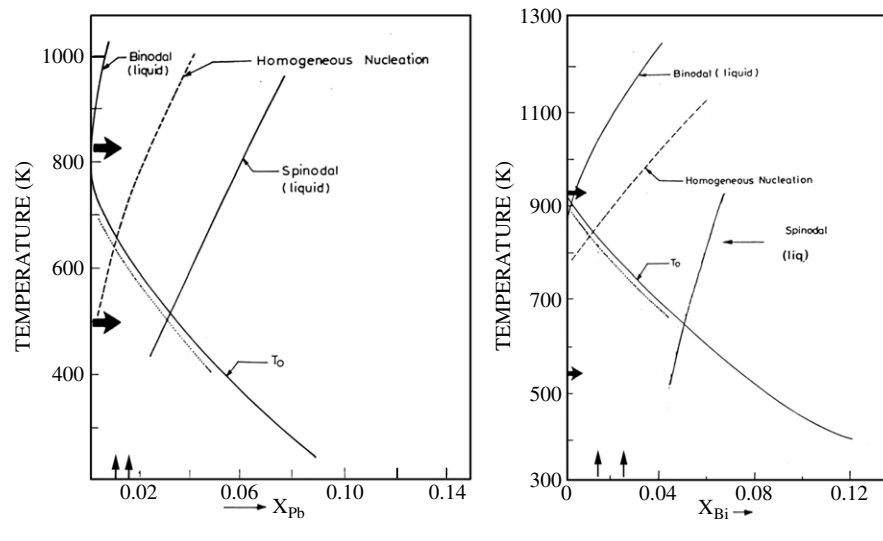
Figure 2: Electron micrograph and corresponding selected area diffraction pattern showing the orientation between the nanoscaled inclusion and aluminium is shown in figure for (a) Pb (b) In (c) Bi (d) Sn.



As pointed out by Cahn and Kalonji,<sup>25</sup> the minimum energy shape is expected to conform to the intersection symmetry of the matrix and the particles in the absence of any external stress. The observed shape of the particles gives us an idea about the solidification pathway the particle has followed. During cooling, the liquid droplets are entrapped by the solid matrix ( $S_1$ ) and the shape changes conforming to the point group symmetry of the matrix. The intersection group of the liquid particles in solid matrix will be the same as the point group of the matrix (as the symmetry of liquid is  $\infty, \infty, \infty$ ) and upon solidification the solid conforms to the same shape assuming a cube-on-cube orientation relationship. In case of Pb and In, we observe cuboctahedral shaped particles. The second sequence bypasses the liquid phase separation leading to solute trapping. In this case a large kinetic undercooling is required for the metastable solid to nucleate and grow at a rapid rate. The metastable solid solution thus obtained decomposes by solid state precipitation or spinodal decomposition. This ensures a fine scale distribution of nanoscaled particles. In case of solid state decomposition, the symmetry of the particle is dictated by the intersection symmetry of the point group of the particle and the matrix. The shape obtained from solid state precipitation can be different from that expected through liquid state separation. In order to evaluate the possible

pathways of the microstructural evolution, one needs to determine by thermodynamic calculations the metastable phase diagram of the system. These include the metastable extrapolation of the binodal and spinodal lines for liquid and a determination of equal free energy curve ( $T_o$ ) between solid and liquid.<sup>26</sup> In addition, one needs to determine the limit set by homogeneous nucleation in case we are evaluating the stability of the liquid during quenching. We present two simple examples of phase diagrams viz. Al-Pb and Al-Bi (shown in figure 3) in order to elucidate the differences in sequence of phase evolution.<sup>27</sup> The envelope bounded by binodal point, homogeneous nucleation line and the equal free energy line mark the region where the liquid can remain metastable and can avoid decomposition. Quenching through this region, it is possible to cross the equal free energy  $T_o$  curve under favorable kinetic condition and form solid solution without any partitioning by the solute trapping process. The liquid with composition lying in the right hand side outside this envelope will decompose spontaneously into two liquids. Thus, the extent of the envelope and the melt composition with respect to the envelope determine whether the dispersed particles will develop through the partitionless solidification and subsequent solid state decomposition or by liquid state decomposition of the melt. Both the compositions chosen in case of Al-Pb (shown in figure 3a) lies to

Figure 3: Phase diagrams calculated using Miedema's model showing metastable extension of liquid phase field (binodal), liquid spinodal and  $T_o$  of liquid and solid solution at the Al rich end. Superimposed on it a dashed line denoting undercooling required for homogeneous nucleation of second liquid ( $l_2$ ). The undercooling required for solute trapping is indicated by a dotted line. Horizontal arrows from top showing monotectic composition and eutectic temperatures and vertical arrows showing alloy compositions studied: (a) Al-Pb (b) Al-Bi.



the right of the envelope. Therefore, in such cases liquid state phase separation occurs and nanoliquid droplets gets trapped within the aluminum matrix. This results in liquid particles with cuboctahedral symmetry. The symmetry remains same as Pb solidifies with a fcc structure and with cube on cube orientation relationship. However, in the case of Al–Bi (see figure 3b), the envelope is wider and it is possible to have partitionless solidification and subsequent decomposition over a relatively larger composition range. The shape of these solid-state precipitates is generally guided by the growth anisotropy. In case the driving force for growth dissipate quickly or the diffusion limits the growth, coarsening sets in and the shape is controlled by the surface energy. For nanometric particles the time required for the equilibration of the particles are small due to their small length scale. In such a case, the shape is dictated by the intersection symmetry. Thus, orientation relations between the particle and the matrix play important role in determining the shape of the particles. And, intersection symmetry depends on the orientation relation. There have been reports suggesting that the particles have wide spread in the orientation relations and different variants nucleating within the same droplet. We have actually observed different OR in case of Al–Sn alloys.

Kim and Cantor<sup>28</sup> studied the orientation relation of Sn dispersoids in aluminum matrix synthesized by rapid solidification.

Although they observed a degree of scatter, the particles are oriented within  $10^\circ$  of the following two orientation relations:

$$\left. \begin{array}{l} [\bar{2}11]_{Al} // [010]_{Sn} \\ \{111\}_{Al} // \{100\}_{Sn}, \end{array} \right\} \quad (1)$$

$$\left. \begin{array}{l} [011]_{Al} // [011]_{Sn} \\ \{100\}_{Al} // \{100\}_{Sn} \end{array} \right\} \quad (2)$$

Johnson et al.<sup>29</sup> confirmed the existence of the orientation relation (2) for ion-implanted Sn dispersions in Al matrix. We also observed the orientation relation (2) for nano-Sn particles with the Al matrix in the Al–Sn binary alloy, which was primarily synthesized for comparison of results with the ternary alloys.

We have also observed different variants nucleate within the droplet. In case of Zn–3.3at%Bi,<sup>30</sup> a bright-field TEM image after the sample has undergone a full thermal cycle, i.e. heating to 570 K and cooling to 360 K, shows polycrystalline Bi particles.

A schematic representation of the diffraction pattern shows that there are 12 particle variants expected in the observed orientation relationship.

This can be understood by invoking the order of intersection point group symmetry and that of the point group symmetry of the matrix. The order of the matrix point group (6/mmm) is 24 and that of the intersection point group ( $-1$ ) is 2. The ratio of the order of the point group symmetry of the matrix and that of the intersection group is the number of variants and therefore, the variants are 12. The grain which nucleates on the particle/matrix interface in the polycrystalline particle will belong to one of 12 variants. There is also a possibility of nucleation at the Bi grain boundaries of the polycrystalline particle.

For cases where we report different orientation relationships, we rule out any unique intersection group and shape. It is therefore, not surprising that we observe particles with many different shapes (see figure 2c). However for the particles, which originally got embedded in the matrix in the liquid state, one sees the remnant of the equilibrium shape between the matrix and the liquid in the form of truncated octahedron shape. For Pb and metastable cubic In with point group  $m\bar{3}m$  and matrix  $m\bar{3}m$ , the symmetry of the particle is  $m\bar{3}m$ . Cube, octahedron and cuboctahedron all exhibit this symmetry. Experimentally we observe these shapes for metastable cubic indium. The variations of shapes are not observed in the case of Pb where cuboctahedron seems to be the predominant shape. The shape observed for the embedded nano particles can be the equilibrium shape. The equilibrium or critical nucleus shape at a macroscopic step is addressed through the Gibbs-wulff construction (minimum surface energy configuration). In the absence of strain energy, the equilibrium shape (i.e., the critical nucleus shape) for a particle in a homogeneous matrix is determined by the Gibbs-Wulff construction.<sup>31,32</sup> Winterbottom<sup>33</sup> has extended this construction to find the equilibrium shape of a liquid drop upon a substrate with the aid of the concept of negative surface tension. In the growth stage, growth kinetics plays a role. The anisotropy of specific surface free energy determines the equilibrium crystal shape, while the growth shape is also affected by the anisotropy of the mobility or kinetic coefficient. Different interface may have different growth kinetics and if growth anisotropy is not there, the equilibrium shape does not alter in growth stage also.

### 2.3.2. Shape of alloy particles

Studies on alloy particles are limited and only in recent times attempts have been made to synthesize such particles. Pb–In alloy particles embedded in aluminum<sup>34</sup> have been investigated. Lead and indium form complete solid solution.

These particles are cuboctahedral in shape and bounded by {111} and {100} facets and exhibits cube on cube orientation relationship with aluminum matrix. In these particles there is a preference for the formation of the 111 interfaces leading to the occasional occurrence of the octahedral shape. The extent of the {100} faceting is so small that it has not been possible to detect the resolution at which we observe the particles. On the otherhand, Pb-Cd inclusions in aluminum matrix (two-phase inclusions) consist of a fcc Pb part forming the segment of a cuboctahedron and a hcp Cd slab attached to one of {111} Pb facets<sup>35</sup>. The close packed planes and directions of the three phases are parallel to each others yielding simple orientation relationship. The two phase Pb–Sn alloy particles embedded in aluminum have been studied by Bhattacharya et al.<sup>36</sup> The Pb in most cases shows a cube on cube orientation relationship with the aluminum matrix. The Sn shows a different orientation relation of  $(2\bar{2}0)\text{Al} // (101)\text{Sn}$  and  $[220]\text{Al} // [020]\text{Sn}$  between Al and Sn (figure 4). In this case the particles were synthesized by rapid solidification. In most of the cases, the overall shape of these embedded nano particles are near cuboctahedral and the relationship among Pb, Sn and Al can be written as

$$\begin{aligned} & (2\bar{2}0)\text{Al} // (2\bar{2}0)\text{Pb} // (101)\text{Sn} \text{ and} \\ & [220]\text{Al} // [220]\text{Pb} // [020]\text{Sn}. \end{aligned}$$

Similarly, In-Sn and Bi-Sn alloy nanoparticles in Al matrix exhibit distorted cuboctahedral symmetry.<sup>37,38</sup> These particles show presence of two phases  $\beta(\text{In}_3\text{Sn})$  and  $\gamma(\text{InSn}_4)$  at nanoscaled. A

study of orientation relationship indicates that the  $\beta$ -phase possess a unique orientation relationship with Al, whereas the  $\gamma$ -phase does not exhibit any unique orientation relationship with the matrix. This is shown in figure 5. Melting studies show significant depression in onset of melting point of the alloy in case of nanoparticles compared to the melting point in bulk alloys. The BiSn two-phase nano particles in Al shows presence of metastable phase and high temperature x-ray and dsc studies show that the metastable phase is associated with large undercooling, The difficulty in nucleating Sn in the embedded particles is proposed to be the main cause for the observation of the metastable Sn-rich phase.<sup>38</sup>

#### 2.4. Defects in the embedded particles and the matrix

There exists limited number of study to unravel defects at the interfaces and inside the nanoembedded particles. The possible defects that can arise from the geometrical effect of constraining cavity have been discussed by Pond et al.<sup>39</sup> In case the particles have the same point group symmetry as that of the matrix, geometrical defects are not necessary to fill the cavity. However, if the point group symmetries are different, defects can exist either at the interface as steps or in the interior as additional interfaces among variants. In case where you have the defect as additional interface, the particle does not remain single crystal any more. The twinned boundaries observed in germanium crystal embedded in aluminum matrix by Gouthama<sup>40</sup> are classical example of such a defect. In case of Pb particles embedded in alloyed matrix of Cu and

Figure 4: A typical micrograph showing presence of bi-phase Pb–Sn inclusions in aluminum.

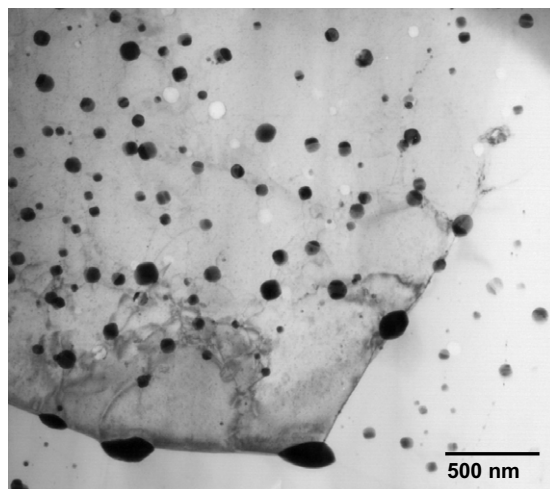
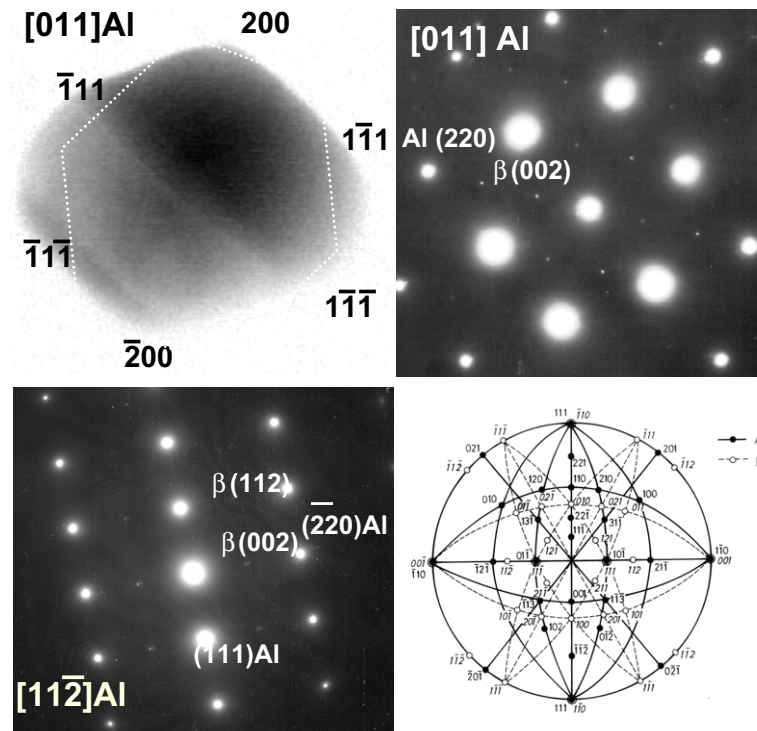


Figure 5: (a) Atypical electron micrograph of In-Sn nanoparticle shows the presence of the beta and gamma phases (b) and (c) SADP shows that the beta phase possess an OR with Al (d) Stereogram depicts the orientation relationship.



Zn with lower zinc concentration, the particles are cuboctahedron in shape bounded by 111 and 100 facets. High-resolution electron microscopy reveals that the particle-matrix interface in the as spun sample contains steps of height 0.42–1.9 nm on the {111} planes<sup>41</sup>. Repeated thermal recycling from room temperature to a temperature above the melting point leads to complete removal of these steps indicating that these stepped structures are of kinetic origin and not geometrical. At small sizes the embedded particles some time exhibit twin or faults particularly if the matrix is rigid. As an example, stacking fault like defects could be observed in lead embedded in amorphous silica matrix<sup>42</sup>. In case of Pb-In alloy particles embedded in aluminum, there is a report of the presence of dislocation loops in the particles.<sup>34</sup> In case of Al–1.8at % (Pb<sub>56</sub>In<sub>44</sub>), the particles retain faceted shape even at 723 K while some of the particles show slow atomic step activity. This is shown in figure 6.

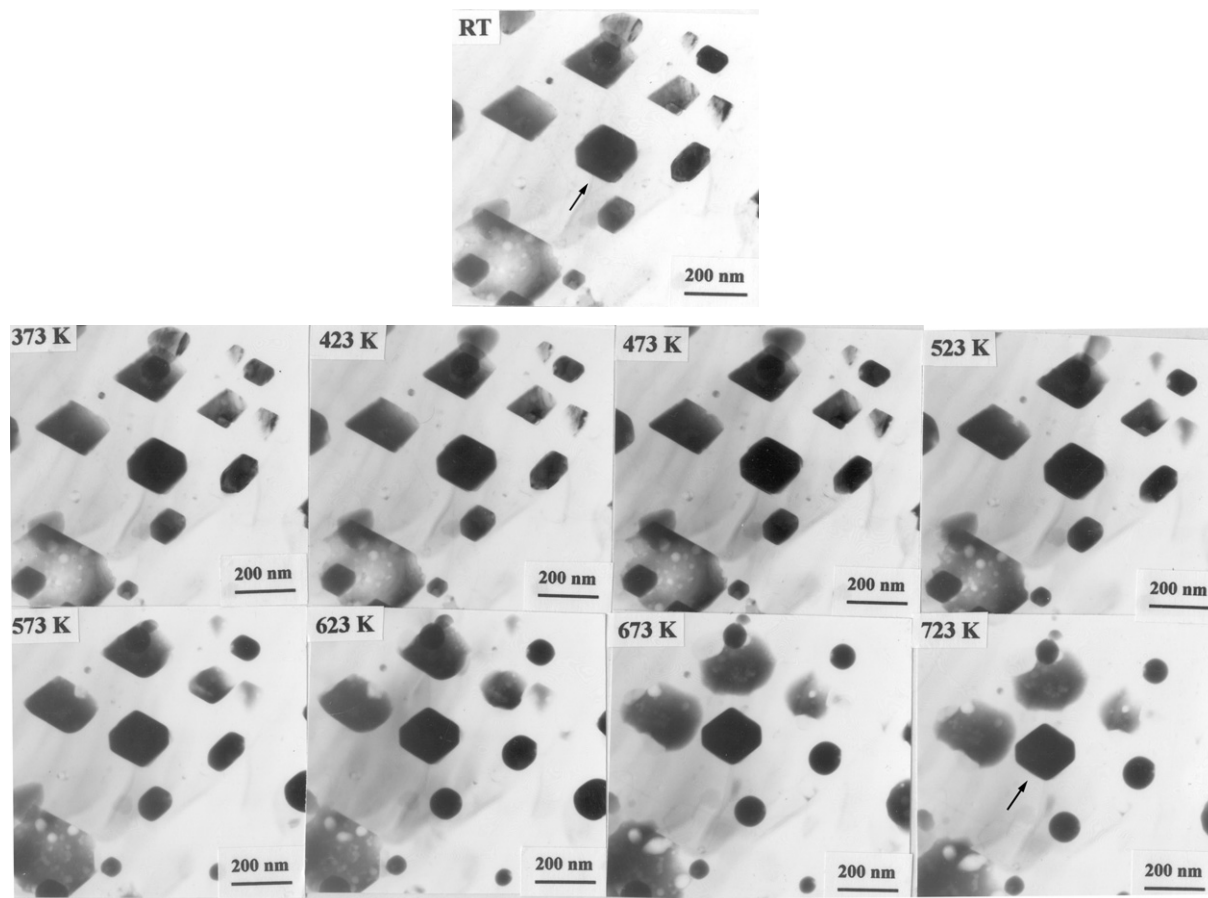
### 3. Transformations in embedded particles

#### 3.1. Shape changes in embedded particles during transformation

The embedded nano particles bounded by sharp interfaces often exhibits superheating during

melting. Careful analysis of the variation of Al–Pb surface-energy anisotropy  $\sigma_{100}/\sigma_{111}$  as a function of temperature from measurements of {100} and {111} facet separation for a series of individual Pb particles in Al matrix indicates that the values have a wide spread in the melt-spun state with the peak at around 1.18.<sup>43</sup> The anisotropy of solid Al–solid Pb surface energy is constant between room temperature and the melting point of Pb, with the {100}<sub>Al,Pb</sub> surface energy about 14% greater than the {111}<sub>Al,Pb</sub> surface energy. The {100}<sub>Al,Pb</sub> facet on solid Pb particles embedded in an Al matrix disappears when the Pb particles melt. The anisotropy of solid Al–liquid Pb surface energy decreases gradually with increasing temperature above the melting point of Pb, with the ratio of {100}<sub>Al,Pb</sub> and {111}<sub>Al,Pb</sub> surface energies falling from about 1.14 to 1 over the temperature range 350–550°C. This increases steadily on thermal recycling of the sample through melting transition and the ratio shifts to 1.3–1.5 indicating the dominance of 111 planes. This is so because along with the annihilation of surface defects, which act as heterogeneous nucleating site for phase change, the facets sharpen and surface energy ratio of the planes are altered. There is a tendency of increasing the

Figure 6: In situ heating sequences in Al- 1.8 at %( $\text{Pb}_{70}\text{In}_{30}$ ) sample shows melting of PbIn nanoparticles. Interestingly, one particle marked in figure does not show roughening even at 723 K



area of 111 facets with lower energy and decreasing defects leading to the emergence of superheating. Immediately after melting, the {100} planes bulge outwards and become rounded whereas the {111} planes remains flat until the temperature reaches around 500°C when the inclusion rapidly becomes spherical. It has been suggested that roughening transition plays a role in such transitions.<sup>44</sup> Gabrisch et al.<sup>45</sup> has focused on the characteristics of the equilibrium shape for small Pb inclusions in Al matrix. They observed a relation between the size and the location in Al matrix. Using high-resolution electron microscopy, they established that unlike the equilibrium shape of free particles, the shape of inclusion changes with size and certain ‘magic sizes’ are preferred.<sup>45</sup> This behavior can be ascribed to the oscillatory nature of strain energy that dominates at small sizes.

In order to characterize the Pb precipitate sizes accurately, the {111} facet pair distances of the precipitates were measured separately from high

resolution micrographs. A histogram of the number of facet pair vs size/number of Al(111) planes shows some unexpected results, that the precipitate sizes were distributed such that some sizes were preferred while others were avoided. This so-called ‘magic’ size effect can be understood as a consequence of the confinement of the Pb precipitates in the solid Al matrix when volume strain is accommodated by matrix vacancies as much as possible. The residual misfit strain, calculated from the atomic plane positions in an undistorted interface, contributes with an oscillating energy term whose periodicity matches the moiré functions between the two lattices and represents the residual misfit strain energy. This phenomenon is referred to as oscillatory nature of strain energy.

In situ-heating experiments on Pb-In nanoparticles embedded in aluminum matrix confirm the kinetic origin of shape of the particles. The results indicate that the behavior can be different from particle to particle. In situ heating experiments

show that while some particles roughened to give spherical shape, there are other particles, which do not exhibit roughening transition for both the 100 and 111 planes. The study also revealed that while few adjacent sets of planes still remains faceted, the planes opposite to them have undergone roughening transition. It suggests that a major role is being played by interfacial segregation during roughening transitions. Since segregation can be different for different particles the roughening behavior can also be different.

### 3.2. Liquid to solid transformation

Considerable interest in studying phase transformation in nanoparticles exists with particular emphasis to liquid to solid transformation. The primary issue is the nucleation behavior of the solid in the entrapped liquid. It has been shown that if the melt is divided into small metal clusters, with no connectivity among them, large super cooling is achievable (Turnbull).<sup>46–48</sup> From the classical nucleation theory by Christian,<sup>49</sup> there exist a barrier to the nucleation of solidification from the melt. The cause of the barrier is the energy spent for the creation of interface associated with the new phase that appears during solidification. Therefore, solidification always occurs below the thermodynamic freezing temperature. Classical nucleation theory predicts that the transformation of super cooled liquid to solid phase can occur homogeneously. However, even in samples quoted to be very pure, certain amount of impurities are always present, and they act as catalyst for heterogeneous nucleation<sup>50</sup> at temperatures much above the homogeneous nucleation temperature. Turnbull have systematically studied undercooling of liquid metals and obtained a maximum undercooling of  $\sim 0.18 T_m$ . It was then inferred that by entraining the droplets in emulsifying liquids, homogeneous nucleation could be achieved. But the later experiments by Southin and Chadwick<sup>51</sup>, and Perepezko<sup>52</sup> succeeded in obtaining a much higher undercooling. Thus, it became clear that most of the Turnbull's results probably correspond to the heterogeneous solidification.

#### 3.2.1. Depression of freezing point

The depression of the freezing point as a function of size has been studied extensively. Buffiat and Borel<sup>53</sup> have developed the thermodynamic criterion to estimate this depression. Recently Sheng et al.<sup>54</sup> and Li et al.<sup>55</sup> have shown a size-dependent freezing behavior for Pb nanoparticles embedded in Al matrix synthesized by mechanical milling. The freezing temperature decreased with increase in milling time for Al–Pb and subsequent reduction

in particle size of incoherent Pb nanoparticles. They have also investigated In, Sn, Bi and Cd nanoparticles in ball milled samples.

Analysis from classical nucleation theory gives us the free energy for homogeneous and heterogeneous nucleation. For bulk liquid freezing below equilibrium freezing point  $T_O$ , this is given by  $\Delta G_v = cL_o \Delta T_f / T_o$  where  $\Delta T_f = T_o - T_f$

However, for particles with radius  $r$ , freezing starts at a different temperature  $T_r$ , and  $\Delta G_v$  should be modified because it is affected by the surface energy change during solidification.<sup>56</sup> After converting the latter into equivalent energy change per unit volume, the driving force for solidification is

$$\Delta G_v = \frac{\rho L_o}{T_o} \Delta T_f + \frac{3\alpha(\sigma_{lm} - \sigma_{sm})}{r} \quad (3)$$

where,  $\alpha$  is a solid-state diffusion parameter with values  $0 < \alpha < 1$  because only a fraction of the liquid/matrix interface is replaced by solid matrix interface upon nucleation.

Maximum  $\Delta G$  is given by the condition,

$$\left( \frac{\partial \Delta G}{\partial R} \right) = 0, \quad (4)$$

$$R^* = \frac{2\sigma_{ls}}{\Delta G_v} \quad (5)$$

According to the classical nucleation theory, the heterogeneous nucleation frequency per droplet is<sup>57</sup>

$$I = N_C \frac{kT}{h} \exp\left(-\frac{\Delta G^*}{kT}\right) \exp\left(-\frac{Q}{kT}\right) \quad (6)$$

where,  $N_C$  = number of nucleation sites per unit volume and  $Q$  = activation energy for transferring atom across liquid-solid interface.

The nucleation frequency  $I$  is determined from  $\Delta G^*$ . The  $\Delta G^*$  contains  $\Delta G_v$  and undercooling,  $\Delta T_r$  for a given particle-matrix system. Both of these are size dependent for small particles system.

It can be shown that

$$\Delta T_r = \Delta T_o + \frac{T_o}{\rho L_o} \frac{3\alpha(\sigma_{sm} - \sigma_{lm})}{r} \quad (7)$$

$\Delta T_r = \Delta T_o + \alpha \Delta T_m$  where  $\Delta T_m = T_o - T_m$  reflects the melting point depression.

Thus, undercooling of nanoparticles is larger compared to the 'bulk materials' or corresponding micrometer counterparts. Nanoparticles with more pronounced melting point depressions shows larger undercooling on freezing as is clear from equation (5). Indeed, such an analysis is supported by interrupted differential scanning

calorimetric thermograms of In nanoparticles embedded in Al produced by mechanical milling. Smaller particles, which melt first on heating, solidify at an undercooling that is larger than the undercooling of the larger particles. Thus, undercooling increases with decrease in particle size and apparent large undercooling is interpreted as a combined consequence of dependence of the need for nucleation of solid and the size-induced melting point depression.

### 3.2.2. *Heterogeneous nucleation of solidification*

Nucleation of solidification of individual droplets has been studied in the presence of clean substrates<sup>58–60</sup> and in the absence of substrate.<sup>61–63</sup> Irreproducible results in supercooling measurements led to the development of entrained droplet technique<sup>64</sup> and its adoption by Southin and Chadwick<sup>51</sup> to the study of solidification of low melting metal in higher melting matrix. Calorimetry, dilatometry and microscopy can be employed to monitor the solidification behavior of these particles. Solidification of such fine droplets generally occurs by a single nucleation event with insignificant growth. In case the calculated critical nuclei size exceeds the size of these embedded liquid droplets, solidification might be bypassed. Droplet solidification is catalysed by epitaxial nucleation on the surrounding matrix and hence is controlled by the matrix and the crystallographic shape of the cavity inside the matrix. Doping of the matrix with trace alloying elements has enabled investigations of the influence of chemistry of droplet-matrix interface on heterogeneous nucleation. The thermodynamic limit to which a liquid can be under cooled ( $0.5–0.75 T_m$ ) was predicted by Kauzmann<sup>65</sup> from the entropic instability. Experimentally, it is found that if the liquid can be cooled by avoiding crystallization, it forms glass between  $0.3–0.75 T_m$ . Singh and Holz<sup>66</sup> gave the estimate of the limit of maximum supercooling that can be obtained from classical nucleation theory for homogeneous nucleation. The reasonable value which comes up from their results is  $\sim 0.56 T_m$ . However, this does not take into account variation of surface energy with temperature. In certain embedded nanoparticles a wide temperature range for solidification could be observed. Undercooling achievable during nucleation of solidification is not directly related to size. However, since the smaller sized particles are expected to contain less impurity, they will have lesser concentration of heterogeneous nucleation sites. Therefore, the smaller particles would solidify later closer to the homogeneous nucleation temperature. Wider

range of particle size distribution, an outcome of the processing route (like melt spinning), is expected to yield a broad range of solidification event. However, broad solidification event is not a reality for all samples produced by melt spinning. There are two important variables that influence the heterogeneous nucleation. These are potency and concentration of nucleation sites. The wetting angle is a measure of the potency of the nucleation site in the framework of classical heterogeneous nucleation theory. A related question is the correctness of the assumption of classical heterogeneous nucleation event. Goswami et al.<sup>26</sup> have shown that number of catalytic nucleation sites  $N_c$  and contact angle  $\theta$  can be estimated for nanodispersed particles from controlled differential scanning calorimetric experiments. Unreasonable low  $N_c$  values are obtained for large number of cases. These results have suggested an apparent breakdown of the classical heterogeneous nucleation theory with hemispherical cap model. However, the later work suggests that the microscopic details of the interface plays an important role in the nucleation process and may have biased the earlier results. The interface in the presence of defects cannot be treated as having a single contact angle. Instead it can be modeled with a spread in contact angle. This gives a reasonable reproduction of the DSC curve using the classical heterogeneous theory as shown by Goswami, et al.<sup>26</sup> In cases where the anisotropy of liquid-solid surface energy is very large, the nanodispersed particles bounded predominantly by low surface energy interfaces can be used to test the classical heterogeneous nucleation theory. Such a study employing dispersion of lead in zinc matrix strongly suggests the validity of the classical theory of heterogeneous nucleation<sup>27</sup>.

### 3.2.3. *Melting behaviour of embedded nanoparticles*

Lindemann<sup>67</sup> had proposed melting as the vibrational instability released when the root mean square amplitude of vibration reaches 10% of interatomic distance (critical value). Experimental observation of surface melting of different crystallographic planes at different temperatures below  $T_m$  and increase in thickness of the melted layer as  $T_m$  is approached supports this criterion<sup>68–70</sup>. Uhlmann<sup>71</sup> had approached the melting phenomena from classical nucleation theory. However there remains no experimental evidence for homogeneous nucleation during melting. Initiation of melting occurs at the solid vapour surfaces and at the internal boundaries of solid. Therefore, heterogeneous nucleation of melting is rather possible. Ever since Lindemann proposed his melting hypotheses, theoretical modifications as

well as experimental tests have been performed by various groups of scientists<sup>70,72</sup>. Based on theoretical analysis and numerical calculations on various metals and rare gases, Cho<sup>73</sup> found that the Lindemann constant and the Lindemann parameter (the critical ratio of vibration amplitude over the interatomic distance) are structure-dependent, i.e. they are significantly different for bcc, fcc and hcp metals and Lindemann law holds for each structure separately. As a one-phase theory, Lindemann criterion is not thermodynamically sound as it does not take the free energy of the liquid state into account<sup>71</sup>. Also, such an approach to understand melting does not explain the mechanism leading to melting. The universality of melting has come to be questioned after superheating has been reported for solid Ar in Al, Ag in Au, Pb in Al.<sup>74–77</sup> Fecht and Johnson<sup>78</sup> have proposed an entropic instability limit to which a metal can be superheated i.e. the temperature at which entropy of solid will be more than that of liquid (inverse Kauzmann temperature).<sup>79</sup> Although, this is the uppermost instability point, there can be other instability limiting the existence of the superheated solid like the shear instability pointed out by Born<sup>80</sup> and volume instability pointed out by Tallon.<sup>81</sup> Born criterion of melting states that as temperature rises, the atomic distances in a solid increase and the restoring force decreases due to thermal expansion. And, therefore the shear modulus of a crystalline solid decreases with an increase in temperature. Born further stated that the difference between a solid and a liquid is that the solid exhibit an elastic resistance against shearing stress while the liquid does not. Hence, Born's criterion was developed as definition of melting in terms of mechanical instability of a crystal: melting of a crystal occurs when one of its shear modulus vanishes. Similar to Lindemann melting criterion, Born's model is also a one-phase theory that contains no distinct description of liquid, and thus fails to account for the discontinuous, first order character of the melting transition. We know that solids usually melt at a temperature below their  $T_o$  due to pre-melting at surfaces or interfaces that act as heterogeneous nucleation sites for melt. When heterogeneous nucleation of melt at surfaces is suppressed, e.g. by means of proper coating with a high- $T_o$  material, melting would occur well above  $T_o$ , which is normally referred as to superheating. Experimental observations showed that superheating can be achieved in various systems including metals and inorganic solids and the degree of superheating is dependent on kinetic factors (such as the heating rate) and structural ones such as the particle sizes and the effectiveness of

coating. An interesting question to be answered is whether there is an ultimate limit for superheating of a solid, which is fundamentally correlated with the mechanism governing the melting of solids. Fecht and Johnson<sup>78</sup> explored the limit of superheating in solids by examining the temperature dependence of entropy change for a superheated solid and liquid, respectively, which is analogous to the famous Kauzmann's paradox in supercooled liquids. Kauzmann<sup>79</sup> noticed that the entropy difference of a crystal and a supercooled liquid may vanish at a temperature well above absolute zero, below which the supercooled liquid would have lower entropy than the crystal. In dealing with superheated solids, Fecht and Johnson<sup>78</sup> pointed out that a similar entropy paradox exists at a temperature well above the  $T_o$  beyond which the entropy of a superheated crystal exceeds that of the liquid. The temperature dependence of entropy for a crystalline and liquid Al for both stable and metastable states are calculated. The isentropic temperature  $T_{sm}$ , also termed as the inverse Kauzmann temperature or F–J temperature, was determined as  $1.38 T_o$  if the vacancy contribution is properly included. Tallon et al.<sup>81</sup> tried to modify Born's initial criterion to obtain a more physically sound theory of melting. They found the shear modulus of solid is a continuous function of dilatation through the melting expansion and falls to zero at the dilatation of the liquid. Thus, they suggested that Born's criterion should be replaced by the following: melting occurs when a solid can transform isothermally to a state of zero shear modulus. According to Tallon et al.,<sup>81</sup> the modified theory becomes a two-phase theory capable of explaining the discontinuous character as well as the heat absorption of melting. In the hole theory of liquids, the elementary mechanism of melting is believed to be connected to the formation of vacancies in solids.<sup>82</sup> Besides vacancies, another type of point defects, namely interstitials, were also considered for interpreting melting, known as the Lennard-Jones-Devonshire model.<sup>83</sup> In this model, melting is viewed as an order–disorder transition resulting from the change of relative atomic positions—positional melting, in which the interaction of normal lattice atoms and self-interstitial atoms plays an important role. The idea to understand melting on basis of dislocations was first propounded by Mott.<sup>84</sup> The dislocation theory of melting has gained much supports from computer simulations as well as experiments. It predicts successfully the features of a first-order transition: the latent heat and the volume change of melting, only that the melting temperature cannot be rationalized exactly. Besides the above melting theories, there are other theories, although less-known, dealing with the instability limits of solids (and even liquids) and their possible correlation with melting.

### 3.2.4. Pressure effects in melting transition of embedded particles

The pressure effect in embedded nanoparticles influences the melting and can arise due to the

- (i) capillarity effect due to the decrease in size (reducing size, melting point decreases)
- (ii) differential thermal expansion between the matrix and the precipitate (effect is less than 1°)
- (iii) change in volume during melting (increases the melting point)

$$T_{ml} / T_o = 1 - \frac{3(\sigma_{sm} / \rho_s - \sigma_{lm} / \rho_l)}{rL_o}$$

where,

- $T_{ml}$  = melting point of the embedded particle
- $T_o$  = bulk melting point
- $\sigma_{sm}$  = solid particle-matrix interfacial energy
- $\sigma_{lm}$  = liquid particle -matrix interfacial energy
- $\rho_s$  = density of solid
- $\rho_l$  = density of liquid
- $L_o$  = latent heat per unit mass
- $r$  = radius of the metal particle

The pressure difference developed because of the mismatch in thermal expansion coefficient as estimated by Spaepen and Turnbull<sup>86</sup>

$$\Delta P = [12(\alpha_p - \alpha_m) \Delta T \mu_m k_p] / (3k_p + 4\mu_m)$$

where,

- $\alpha_p$  = linear thermal expansion coefficient of the particle
- $\alpha_m$  = linear thermal expansion coefficient of the matrix
- $k_p$  = bulk modulus of the precipitate
- $\mu_m$  = shear modulus of the matrix

### 3.2.5. Pressure effects on superheating

Considering all the possible pressure effects, we have tried to estimate the maximum superheating that can be observed experimentally for the case of Pb embedded in Al matrix. Table 1 summarizes the results for superheating of Pb obtained for different fcc matrices. The superheating

Table 1: Calculations showing change in temperature obtained due to different contributions, \ affecting the melting point of Pb in different matrices.

	Volume	Thermal	Size	Total $\Delta T$ (calc.)	$\Delta T$ (expt.)
Al-Pb	17	4	54 (10)	75	103
Cu-Pb	17	14	48 (25)	79	125
Ni-Pb	17	26	53 (30)	96	-45

estimated in the case of Al is far below the experimentally observed superheating.<sup>87</sup> Therefore, it is concluded that the interfaces influence the kinetics of melting significantly. The positive sign indicates an increase in melting point. The fourth column indicates the cumulative effect and the numbers in the fifth column indicate the effective superheating/depression of melting point corresponding to observed values for the melt spun alloys when the pressure effects are taken into consideration.

Little attention, however, is paid to understand the influence of the crystallographic shape on melting. There exist results for embedded Pb and Bi<sup>88,89</sup> that suggest shape dependent superheating ability. It has been found that on heat treatment, though the bounding planes do not change, superheating is observed. In case of Bi and Sn particles we do not observe any superheated peak. It is clear that the shape of the particles and the nature of the interface with the matrix play an important role in the transformation behavior of the nanoembedded particles.

## 4. Conclusions

In this article, we have tried to give an overview of our current understanding of nanoembedded particles of metals and alloys with emphasis on synthesis, structure and stability. These types of materials have very wide applications, which include catalysis, spintronics, and giantmagnetoresistance applications. There is a potential for these materials to develop additional functional properties making them prime candidates as small materials.

## Acknowledgement

The present work derives financial support from the Institute and Department of Science and Technology, Govt. of India.

Received 23 October 2008; revised 31 December 2008.

## References

1. H. Gleiter, *Acta mater. (Millenium-Issue)* 48, 1 (2000)
2. H. Gleiter, *Nanostruct. Mater.*, 6, 3 (1995)
3. H. Gleiter, *Prog. Mater. Sci.*, 33, 223 (1998)
4. U. Herr, J. Jing, U. Gonser, and H. Gleiter, *SolidSt. Commun.*, 76, 192 (1990)
5. J. Petermann, *Bull. Inst. chem. Res. Kyoto University*, 69, 84 (1991)
6. H. Johns, in "Rapid Solidification of Metals and Alloys", Monograph No: 8, Institute of Metallurgists, London, (1982)
7. R.W. Cahn, in "Materials Science and Technology" (R. W. Cahn, P. Hassen, and E. J. Kramer, eds.), VCH Publishers, Weinheim, Germany, 9, 493 (1991)
8. R. Nagrajan, and K. Chattopadhyay, *Acta Metall. Mater.*, 42, 947 (1994)
9. A. L. Greer, *Nature* 368, 688 (1994)
10. J. S. Benjamin, *Sci. Am.*, 234(5), 40 (1976)
11. C. Suryanarayana, *Metals and Materials*, 2, 195 (1996)

12. M. O. Lai and L. Lu, *Mechanical Alloying*, Boston, MA, Kluwer Academic Publishers, 1998
13. B. S. Murty and S. Ranganathan, *Intern. Mater. Rev.*, 43, 101 (1998)
14. C. C. Koch and Y. S. Cho, *Nanostructured Materials*, 1, 207 (1992)
15. C. Suryanarayana, *Prog. Mat. Sci.*, 46, 1 (2001)
16. C. J. Brinker and G. W. Scherer, "Sol-Gel Science", Academic Press, Boston, (1990)
17. L. L. Herch and J. K. West, *Chemical Review*, 90, 3 (1990)
18. C. N. R. Rao, *Mat. Sci and Engg. B*, 18, 1 (1993)
19. P. Bhattacharya and K. Chattopadhyay, *Mater. Trans. JIM*, 39, 75 (1998)
20. P. Bhattacharya and K. Chattopadhyay, *Proc. International Conference on Recent Advances in Metallurgical Processes II*, Bangalore India (1997)
21. R. Goswami and K. Chattopadhyay, *Mater. Sci. Engg. A*, 179/180, 163 (1994)
22. J. W. Cahn, *J. Am. Cer. Soc.* 52, 118 (1969)
23. D. R. Uhlmann, B. Chalmer and K. A. Jackson, *J. Appl. Phys.*, 35, 2986 (1964)
24. R. Goswami and K. Chattopadhyay, *Acta Metall. Mater.*, 42, 383 (1994)
25. J. W. Cahn and G. Kalonji, (1982), *Proc. International Conference on Solid to Solid Phase Transformations* The Metallurgical Society of AIME 3
26. R. Goswami, K. Chattopadhyay, W. T. Kim and B. Cantor, *Metall. Trans. 23A*, 3207 (1992)
27. R. Goswami and K. Chattopadhyay, *Phil. Mag. Lett.*, 72, 411 (1995)
28. W. T. Kim and B. Cantor, *J. Mater. Sci.*, 26, 2868 (1991).
29. E. Johnson, C. R. H. Bhal, V. S. Touboltsev, and A. Johansen, in *Nucleation and Growth Processes in Materials*, edited by A. Gonis, P. E. A. Turchi, and A. J. Ardell (Mat. Res. Soc. Sym. Proc., 580, Warrendale, PA, 2000), p. 177
30. R. Goswami and K. Chattopadhyay, *Acta Materialia*, 52, 19, (2004), 5503
31. C. Herring, in: *Structure and Properties of Solid Surfaces*, Eds. R. Comer and C. S. Smith (Univ. of Chicago Press, 1953) p. 5.
32. W. W. Mullins, in: *Metal Surfaces: Structure, Energetics and Kinetics*, Eds. R. Gamer and N.A. Gjostein (ASM, Metals Park, Ohio, 1963) p. 17.
33. W.L. Winterbottom, *Acta Met.*, 15 (1967) 303.
34. P. Bhattacharya; K. Chattopadhyay, *International Journal of Nanoscience*, 4, 909 (2005)
35. E. Johnson, A. Johansen, L. Sarholt and U. Dahmen, *J. Met. Nano. Cryst. Mat.*, 10, 267 (2001)
36. P. Bhattacharya, V. Bhattacharya and K. Chattopadhyay, *J. Mater. Res.*, 17, 11, 2875 (2002)
37. V. Bhattacharya and K. Chattopadhyay, *Materials Science and Engineering A*, 375–377, 932 (2004)
38. Victoria Bhattacharya, E. Yamasue, K. N. Ishihara, K. Chattopadhyay, *Acta Materialia*, 53, 17, 4593 (2005)
39. R. C. Pond and D. S. Vlachavas, *Proc. Roy. Soc. Lond.*, A386, 95 (1983)
40. Gouthama, Ph.D thesis, Department of Metallurgy, Indian Institute of Science, (1989)
41. R. Goswami, K. Chattopadhyay and P. Ryder, *Acta mater.*, 46, 4257 (1998)
42. P. Bhattacharya and K. Chattopadhyay, *Mater. Trans. JIM*, 39, 75 (1998)
43. K. I. Moore, K. Chattopadhyay, and B. Cantor, *Proc. Roy. Soc. Lond. A*414, 499 (1987)
44. R. Goswami and K. Chattopadhyay, *Progress in Mater. Sci.*, 42, 287 (1997)
45. H. Gabrisch, L. Kjeldgaard, E. Johnson and U. Dahmen. *Acta Mater.*, 49, 4259 (2001)
46. D. Turnbull, *J. Appl. Phys.*, 20, 817 (1949b)
47. D. Turnbull, *J. Chem. Phys.*, 18, 198 (1950a)
48. D. Turnbull, *J. Appl. Phys.*, 21, 1022 (1950b)
49. J. W. Christian, *The theory of Phase Transformation in Metals and Alloys* (Oxford, Pergamon Press, 1975).
50. D. L. Zhang, K. Chattopadhyay and B. Cantor, *J. Mater. Sci.*, 26, 1531 (1991)
51. R. T. Southin and G. A. Chadwick, *Acta Metall.*, 26, 223 (1978)
52. J. H. Perepezko, *Mater. Sci. Engg.*, 65, 125 (1984)
53. Ph. Buffiat and J. P. Borel, *Phys. Rev. A*13, 2287 (1976)
54. H. W. Sheng, K. Lu and E. Ma, *Acta mater.*, 46, 14, 5195 (1998)
55. Y. Li, S. C. Ng, Z. P. Lu, Y. P. Feng and K. Lu, *Phil Mag. Lett.*, 78, 1, 37 (1998)
56. G. L. Allen, W. W. Gile, W. A. Jesser, *Acta Metall.* 28, 1695 (1980)
57. G. L. Allen, R. A. Bayles, W. W. Gile, W. A. Jesser, *Thin Solid Films*, 144, 297 (1986)
58. J. H. Holloman and D. Turnbull, *J. Metals Trans AIME*, 803 (1951)
59. B. E. Sundquist and L. F. Mondolfo, *Trans. Metal. Soc. AIME*, 221, 157 (1961)
60. M. Stowell, T. Law and J. Smart, *Proc. Roy. Soc. Lond.*, 318, 231 (1970)
61. L. Lacy, M. B. Robinson and T. Z. Rathz, *J. Crys. Growth*, 51, 47 (1981)
62. A. J. Drehman and D. Turnbull, *Scripta Metall.*, 15, 543 (1981)
63. A. J. Drehman and A. L. Greer, *Acta. Metall.* 32, 323 (1984)
64. C. C. Wang and C. S. Smith, *Trans. Metall. Soc. A.I.M.E.* 188, 156 (1950)
65. W. Kauzmann, *Chem. Rev.*, 43, 219 (1948)
66. H. B. Singh and A. Holz, *Solid State Communications*, 45, 985 (1983)
67. F. A. Lindemann, *Phys. Z.*, 11, 609 (1910)
68. J. W. M. Frenken and J. F. Van der Veen, *Phys. Rev. Lett.*, 54, 134 (1985)
69. J. W. M. Frenken, P. M. J. Maree and J. F. Van der Veen, *Phys. Rev.*, B34, 7506 (1986)
70. D. C. Wallace, *Proc Roy Soc London A*, 433, 631 (1991)
71. D. R. Uhlmann, *J. Non-crystalline Solids*, 41, 347 (1980)
72. J. Maddox, *Nature*, 323, 485 (1986)
73. S. A. Cho, *Phys F: Met Phys*, 12, 1069 (1982)
74. C. J. Rossouw and S. E. Donnelly, *Phys. Rev. Lett.*, 55, 2960 (1985)
75. J. Dages, H. Gleiter and J. H. Perepezko, *Phys. Lett. A*, 119, 79 (1986)
76. L. Graback and J. Bohr, *Phys. Rev. Lett.*, 64, 934 (1990)
77. D. L. Zhang and B. Cantor, *Acta. Metall. Mater.*, 39, 1595 (1991)
78. H. J. Fecht and W. L. Johnson, *Nature*, 334, 50 (1988)
79. W. Kauzmann, *Chem. Rev.*, 43, 219 (1948)
80. M. Born, *J. Chem. Phys.*, 7, 591 (1939)
81. J. L. Tallon, *Nature*, 342, 658 (1989)
82. T. Gorecki, *Z Metall.*, 67, 269 (1976)
83. J. E. Lennard, A.F. Devonshire, *Proc Roy Soc London A*, 167, 317 (1939)
84. N.F. Mott, *Proc Roy Soc London A*, 215, 1 (1952)
85. P. R. Couchman and W. A. Jesser, *Phil. Mag.*, 35, 787 (1977)
86. F. Spaepen and D. Turnbull, *Scripta Metall.*, 13, 149 (1979)
87. R. Goswami and K. Chattopadhyay, *Acta Mater.*, 43, 7, 2837 (1995)
88. S. J. Peppiat and J. R. Sambles, *Proc. Roy. Soc. A*345, 387 (1975)
89. G. D. T. Spiller, *Phil. Mag. A* 469, 535 (1982)



**Kamanio Chattopadhyay** obtained Ph.D (1978) from Banaras Hindu University, Varanasi. He is presently working as the chairman and a Professor in the Department of Materials Engineering, Indian Institute of Science, Bangalore and convenor of the nanoscience Initiative of the institute. He has published more than 250 research publications in the area of nanoscience and technology, phase transformation, nonequilibrium processing and alloy developments.



**Victoria Bhattacharya** obtained her Ph.D (2006) in Materials Engineering from the Indian Institute of Science. She is presently working as a Research Scientist in Jawaharlal Nehru Centre for Advanced Scientific Research.